UC San Diego
UC San Diego Previously Published Works

Title

Hubbard Nonequilibrium Green's Function Analysis of Photocurrent in Nitroazobenzene Molecular Junction

Permalink

https://escholarship.org/uc/item/3dv0r0mj

Journal

The Journal of Physical Chemistry Letters, 10(7)

ISSN

1948-7185

Authors

Miwa, Kuniyuki
Najarian, Amin Morteza
McCreery, Richard L
et al.

Publication Date

2019-04-04

DOI

10.1021/acs.jpclett.9b00270

Peer reviewed

Hubbard NEGF Analysis of Photocurrent in Nitroazobenzene Molecular Junction

Kuniyuki Miwa,[†] Amin Morteza Najarian,[‡] Richard L. McCreery,[‡] and Michael Galperin[*,†]

†*Department of Chemistry and Biochemistry, University of California San Diego, La Jolla, CA 92034, USA*

‡*Department of Chemistry, University of Alberta, Edmonton, Canada*

E-mail: migalperin@ucsd.edu

Phone: +1-858-246-0511

Abstract

We present combined experimental and theoretical study of photo-induced current in molecular junctions consisting of monolayers of nitroazobenzene oligomers chemisorbed on carbon surfaces and illuminated by UV-Vis light through a transparent electrode. Experimentally observed dependence of the photocurrent on light frequency, temperature and monolayer thickness is analyzed within first principles simulations employing the Hubbard NEGF diagrammatic technique. We reproduce qualitatively correct behavior and discuss mechanisms leading to characteristic behavior of dark and photo-induced currents in response to changes in bias, frequency of radiation, temperature and thickness of molecular layer.

The interaction of light with molecules is an important field of research due to its ability to provide information on molecular structure and dynamics, and to serve as a control tool for intra-molecular processes. Development of nano-fabrication and optical techniques

1

at nanoscale led to tremendous progress in ability to detect and manipulate molecules on surfaces and in junctions. The main signal reported in the literature for devices consisting of molecules attached to macroscopic leads for a long time was current-voltage (conductance-voltage) characteristics.[1–6] Later, standard junction spectroscopies (such as resonant[7,8] and off-resonant[9–13] inelastic electron tunneling spectroscopy) were complemented by probing molecular conduction junctions by optical means.[14–23] For single-molecule junctions the latter is possible only by local electromagnetic field enhancement associated with plasmon excitations.[24,25] Recent developments include observation and optical control of current[26–28] noise,[29,30] and energy transfer.[31,32] Time-dependent and transient effects in junctions observed with optical means,[33–36] tip-enhanced Raman spectroscopy,[37–40] pump-probe spectroscopy in nanojunctions,[41,42] and reporting quantum interference effects[43,44] are also among recent developments. Optical spectroscopy yields a way to estimate heating in current carrying junction[18,19,45,46] Recently, multidimensional spectroscopy measurements in the presence of current (although not yet in junctions) were reported in the literature.[47–49] Optical effects have been also reported in large-area molecular junctions, including internal photoemission,[50] optical modulation of conductance,[51] light emission,[52–55] and photocurrents induced by light absorption.[56,57] Experimental capabilities to study radiation field interaction with molecular conducting junctions gave rise to new branch of nanoscale research - *molecular optoelectronics*[58,59]

Theoretically, challenges in describing optical response in molecular junctions include necessity to account for open character of the system which requires simultaneous treatment of optical transitions in the molecule and electron transfer between molecule and contacts. Single particle language utilized in majority of ab initio studies in molecular electronics usually in the framework of the nonequilibrium Green functions (NEGF) makes it inconvenient to account for differences between transport and optical gaps in junctions. A possible alternative is utilization of molecular many-body states as a basis of consideration. In junctions, such consideration requires utilization of one of many-body flavors of the NEGF. In particular,

2

recently introduced by us diagrammatic technique for the Hubbard NEGF[60] yields a stable and accurate many-body method[61] conveniently suited for description of optoelectronic devices.[59]

Here, we apply the methodology to perform first principles simulation of optical response of recently reported large area nitroazobenzene molecular junctions. Illumination by UV-Vis light induces major changes in current-voltage response, with orders of magnitude changes in conductance and distinct bias dependence compared to the dark behavior.[56] Below after introducing theoretical model and calculational procedure, we present results of first principles simulations and compare them with corresponding experimental data. We then discuss possible mechanisms for changes in dark and photo-induced currents in response to bias, temperature, light frequency, and thickness of the molecular layer.

We consider a nitroazobenzene molecule (see Fig. 1a), M, bridging two metal electrodes, L and R, and subjected to an external laser radiation, rad. The Hamiltonian of the junction is

$$\hat{H} = \hat{H}_M + \sum_{B=L,R,rad} \left(\hat{H}_B + \hat{V}_B \right) \tag{1}$$

Here H_M and H_B are respectively Hamiltonians of molecule and baths, and V_B introduces coupling between them. We represent molecular Hamiltonian $\hat{H}_M$ as a tight-binding chain of N molecular units (see Fig. 1d)

$$\hat{H}_M = \sum_{n=1}^{N} \hat{H}_M^{(n)} + \sum_{n=1}^{N-1} \left(\hat{V}_M^{(n,n+1)} + H.c. \right) \tag{2}$$

For simplicity, we consider all the units to be identical. We represent molecular unit Hamiltonian $\hat{H}_M^{(n)}$ in terms of many-body states $|S_n\rangle$ of the unit. In particular, we consider ground, $|N_g\rangle$, and excited, $|N_x\rangle$, states of neutral molecular unit as well as ground states of anion $|A_g\rangle$ and cation $|C_g\rangle$. First-principle calculations (see Supporting Information for details)

(a)

: C   : O

: N   : H

(b)   (c)

e^-

conductor

$\Delta E = \Delta_M - \mu$ $\Delta E = \Delta_O$

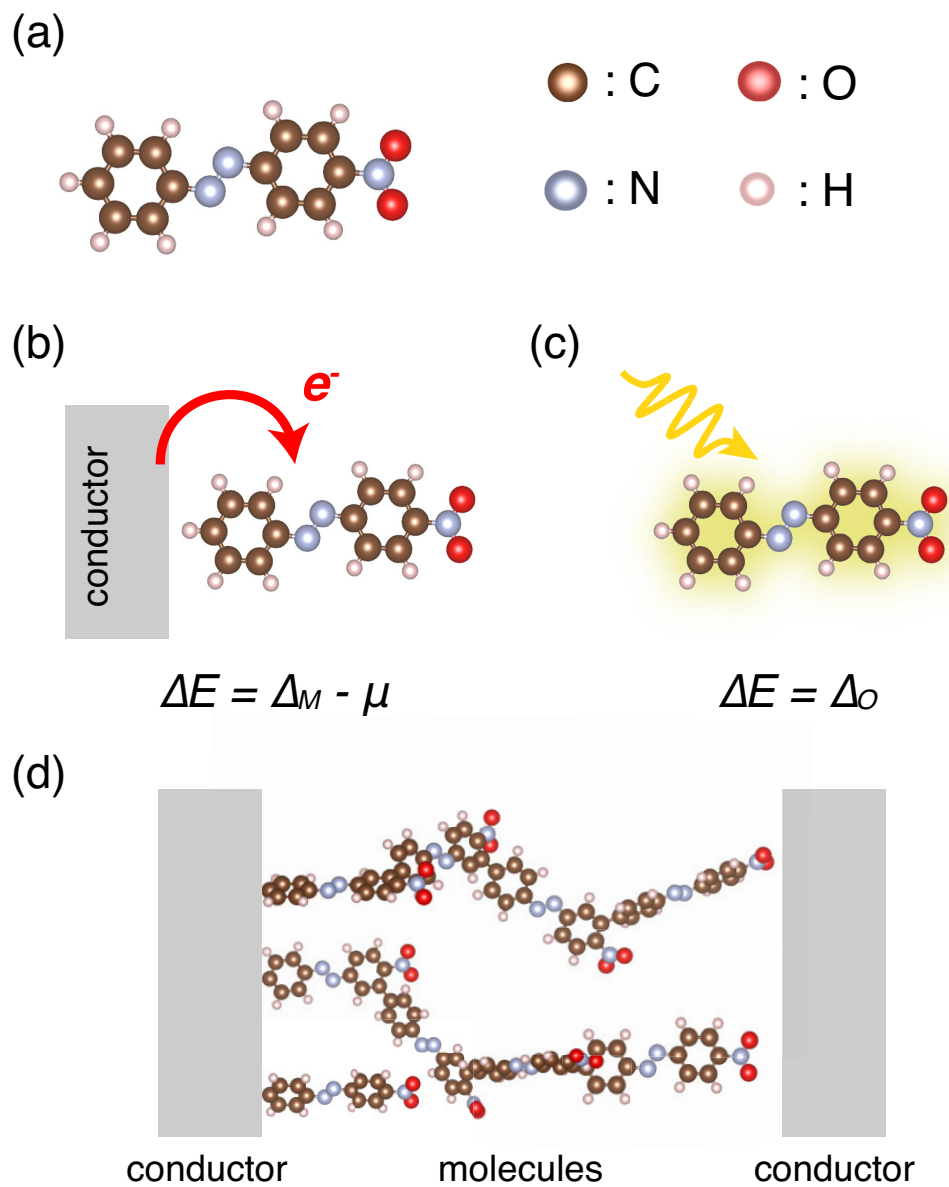(d)

conductor   molecules   conductor

Figure 1: Nitroazobenzene molecular junction. Shown are (a) molecule and sketches of (b) electron transfer process between molecule and contact and (c) optical excitation by external radiation field. Panel (d) sketches molecular chains in the junction.

yield energies of the states E_{S_n}, and explicit form of molecular Hamiltonian is

$$\hat{H}_M^{(n)} = \sum_{S_n \in M_n} E_{S_n} \hat{X}_{S_n S_n} \tag{3}$$

where M_n is molecule n in the chain and $\hat{X}_{S_n S_n} \equiv |S_n\rangle\langle S_n|$ is the Hubbard (or projection) operator.

Contacts are modeled as reservoirs of free electrons each at its own equilibrium

$$\hat{H}_K = \sum_{k \in K} \varepsilon_k \hat{c}_k^\dagger \hat{c}_k \qquad (K = L, R) \tag{4}$$

and radiation field is described as continuum of modes with one mode corresponding to laser frequency populated while all other modes empty

$$\hat{H}_{rad} = \sum_\alpha \omega_\alpha \hat{a}_\alpha^\dagger \hat{a}_\alpha \tag{5}$$

Here $\hat{c}_k^\dagger$ ($\hat{c}_k$) and $\hat{a}_\alpha^\dagger$ ($\hat{a}_\alpha$) creates (annihilates) electron is state k of the contacts and mode α of the field, respectively.

Within each molecular unit we consider four electron transitions (see Fig. 1b) $ET = A_g \to N_g$, $A_g \to N_x$, $N_g \to C_g$, and $N_x \to C_g$ ($\Delta_{ET} = E_{A_g} - E_{N_g}$, $E_{A_g} - E_{N_x}$, $E_{N_g} - E_{C_g}$, $E_{N_x} - E_{C_g}$) and one optical transition (see Fig. 1c) $OT = N_x \to N_g$ ($\Delta_{OT} = E_{N_x} - E_{N_g}$). So that, electron transfer between the units is

$$\hat{V}_M^{(n,n+1)} = \sum_{ET_n \in M_n} \sum_{ET_{n+1} \in M_{n+1}} \left(t_{ET_n, ET_{n+1}} \hat{X}_{ET_n}^\dagger \hat{X}_{ET_{n+1}} + H.c. \right) \tag{6}$$

where ET_n are electron transfer transitions in M_n. First molecule of the chain, $n = 1$, is

coupled to contact L, while last, $n = N$, couples the chain to contact R

$$\hat{V}_K = \sum_{\ell \in L} \sum_{ET_1 \in M_1} \left(V_{\ell,ET_1} \, \hat{c}_\ell^\dagger \, \hat{X}_{ET_1} + H.c. \right) \tag{7}$$

$$+ \sum_{r \in R} \sum_{ET_N \in M_N} \left(V_{r,ET_N} \, \hat{c}_r^\dagger \, \hat{X}_{ET_N} + H.c. \right) \tag{8}$$

$$\hat{V}_{rad} = \sum_{n=1}^{N} \sum_\alpha \sum_{OT_n \in M_n} \left(U_{\alpha,OT_n} \, \hat{a}_\alpha^\dagger \, \hat{X}_{OT_n} + H.c. \right) \tag{9}$$

Our central object of interest is current through the junction caused by either applied bias ($V_{sd} = \mu_L - \mu_R$), or laser field, or both - correspondingly, dark, optical, and total fluxes. Current is introduced as rate of change of the population on the contacts, $I_K = d_t \sum_{k \in K} \langle \hat{c}_k^\dagger(t) \hat{c}_k(t) \rangle$, and at steady-state considered here currents across L and R junction interfaces are equal (with opposite sign), $I_L = -I_R$. Explicit current expression is given by the celebrated Meir-Wingreen formula[62]

$$I_K = \frac{e}{\hbar} \mathrm{Tr} \int \frac{dE}{2\pi} \left(\sigma_K^<(E) \, \mathbf{G}^>(E) - \sigma_K^>(E) \, \mathbf{G}^<(E) \right) \tag{10}$$

where trace is over electronic transitions ET and $\sigma_K^{<(>)}(E)$ and $\mathbf{G}^{<(>)}(E)$ are the Fourier transforms of the lesser (greater) projections of electronic self-energy due to coupling to contact K and Hubbard Green's function, respectively. On the Keldysh contour the correlation functions are defined as

$$[\sigma_K(\tau_1, \tau_2)]_{ET_i, ET_j} = \sum_{k \in K} V_{ET_i,k} \, g_k(\tau_1, \tau_2) \, V_{k,ET_j} \tag{11}$$

$$G_{ET_i,ET_j}(\tau_1, \tau_2) = -i \langle T_c \, \hat{X}_{ET_i}(\tau_1) \, \hat{X}_{ET_j}(\tau_2) \rangle \tag{12}$$

Here $\tau_{1,2}$ are the contour variables, T_c is the contour ordering operator, and $g_k(\tau_1, \tau_2) \equiv -i \langle T_c \, \hat{c}_k(\tau_1) \, \hat{c}_k^\dagger(\tau_2) \rangle$ is the Green's function for free electron in state k.

While explicit expressions for projections of the self-energy are known, Green's function

6

has to be evaluated by solving a modified Dyson equation on the Keldysh contour. Because the Hubbard GF both depends and defines its self-energies, one has to solve the Dyson equation self-consistently until convergence (see Supporting Information and Refs. [60,61] for details).

Unless stated otherwise, simulations are performed at temperature $T = 300$ K. *Ab initio* (TD)DFT calculations of an isolated molecular unit yield electronic transitions $\Delta_{N_g C_g} = -3.5$ eV, $\Delta_{N_x C_g} = -0.08$ eV, $\Delta_{A_g N_g} = -0.11$ eV, $\Delta_{A_g N_x} = 3.31$ eV, while optical gap is $\Delta_{OT} = 3.41$ eV. Strength of molecule-contacts coupling is characterized by escape rate matrix

$$\Gamma^K_{ET_i, ET_j}(E) \equiv 2\pi \sum_{k \in K} V_{ET_i, k} V_{k, ET_j} \delta(E - \varepsilon_k) \qquad (13)$$

which within assumed here wide band approximation does not depend on energy. Simulations are performed for $\Gamma^L_{ET_i, ET_j} = 0.9$ eV and $\Gamma^R_{ET_i, ET_j} = 0.3$ eV for $ET_{i,j} \in \{A_g \rightarrow N_x, N_g \rightarrow C_g\}$ and $\Gamma^L_{ET_i, ET_j} = 0.6$ eV and $\Gamma^R_{ET_i, ET_j} = 0.6$ eV for $ET_{i,j} \in \{A_g \rightarrow N_g, N_x \rightarrow C_g\}$, which are taken to reproduce experimental data (see also Supporting Information). Radiation field is assumed to be coupled to individual molecular units only. Strength of the coupling to radiation field is characterized by dissipation rate

$$\gamma_{OT_n}(\omega) \equiv 2\pi \sum_{\alpha} U_{OT_n, \alpha} U_{\alpha, OT_n} \delta(\omega - \omega_\alpha) \qquad (14)$$

Its frequency dependence is taken from experimental data (see Fig. 2a) with value at molecular resonance, $\omega = \Delta_{OT_n}$, chosen 1.4×10^{-4} eV. Fermi energy is taken as an origin, $E_F = 0$, and bias is applied symmetrically: $\mu_L = E_F + |e|V_{sd}/2$ and $\mu_R = E_F - |e|V_{sd}/2$. Simulations were performed on energy grid spanning range from -16.384 to 16.384 eV with step 2 meV. Convergence was assumed to be reached when populations of the many-body states at subsequent steps of the self-consistent procedure differ by less than 5×10^{-4}.

We first consider photo-induced flux in the absence of bias. Here, we employ single molecular unit model, $N = 1$, in the analysis. Optical excitation promotes electronic population
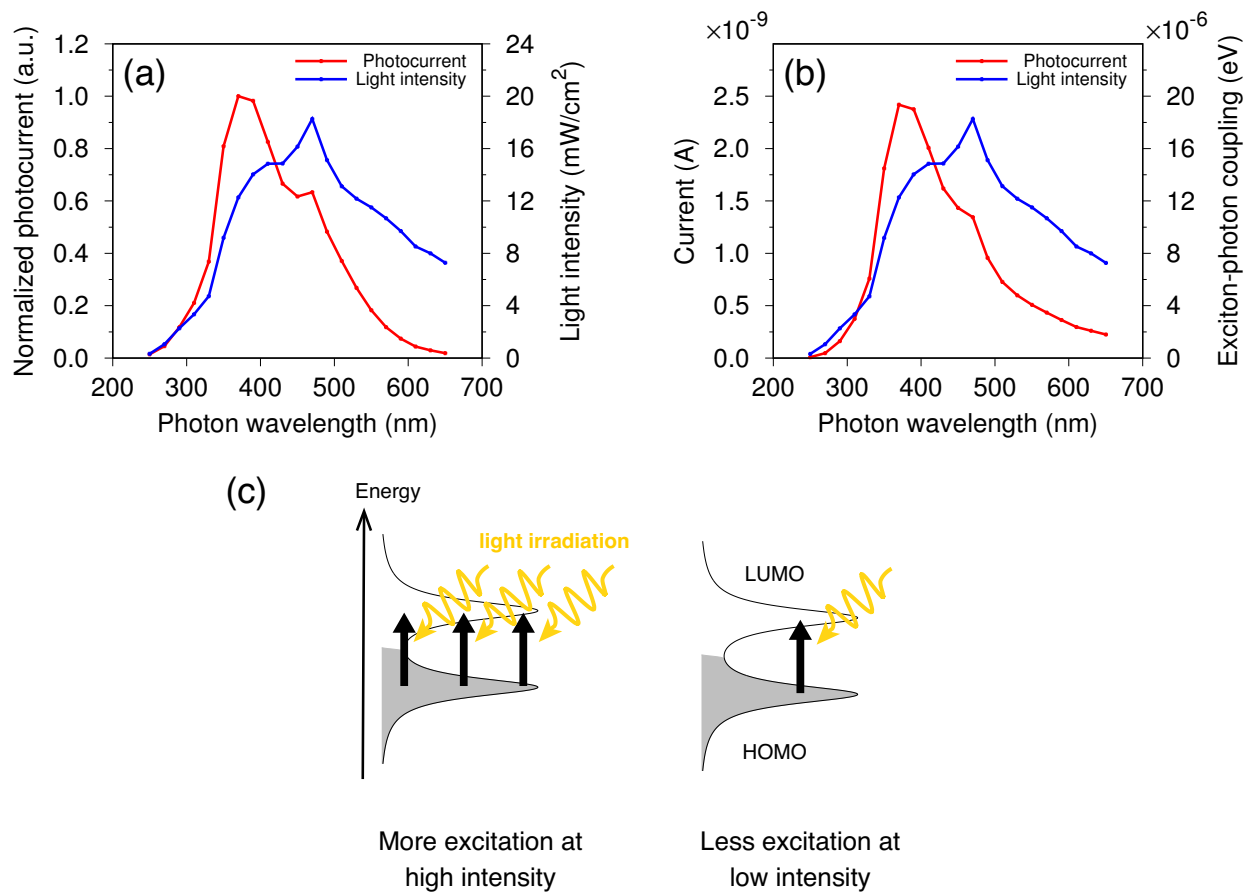
Figure 2: Photocurrent (red line) and light intensity (blue line) as function of radiation field wavelength. Shown are (a) experimental data and (b) theoretical photocurrent resulting from first-principles simulations within the Hubbard NEGF. Panel (c) shows sketch of the mechanism. See text for parameters.

from ground to excited state, then electron either relaxes back or escapes into contacts. Asymmetric coupling of excited state leads to appearance of directed flux even in absence of bias. Figure 2 compares experimental data (panel a) with first principles calculation (panel b). Experimental data for light intensity (blue line) was used as an input in the calculations. As expected, photocurrent shows maximum at frequency corresponding to optical transition Δ_{OT} (panel c). Such light-induced transport was discussed in theoretical literature within simple model considerations.[63] Shoulder observed at longer wavelengths is associated with peak in light intensity at this frequency. One sees qualitative correspondence between experimental data and theoretical simulations.
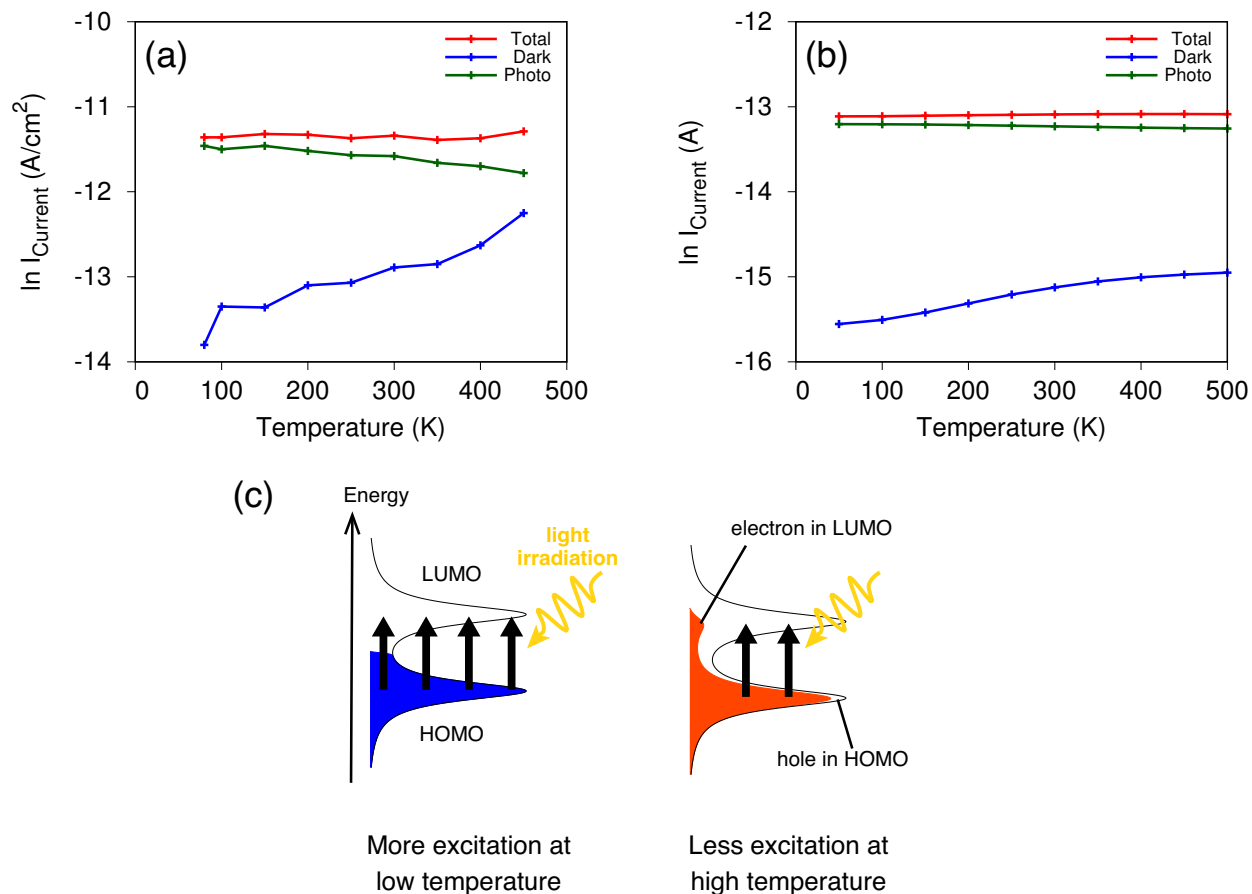

Figure 3: Dark (blue line), photo-induced (green line), and total (red line) currents vs. temperature of the junction. Shown are (a) experimental data and (b) results of first-principles simulations within the Hubbard NEGF. Panel (c) shows sketch of the mechanism. See text for parameters.

9

We now turn to consideration of temperature dependence of current. Also here single molecular unit model, $N = 1$, is enough to describe the observed physics Here junction is subjected to bias of $V_{sd} = 0.02$ eV and measurements are performed in the absence of external radiation (dark current) and under radiation of $\lambda = 380$ nm. With temperature increase the experimental data (see Fig. 3a) show an increase in dark current. At the same time, photo-current (defined as difference between total and dark fluxes) decreases. We note that in the experiment dark current is caused by off-resonant tunneling, while radiation transfers electronic population from ground to excited state in near resonance conditions. Thus plausible mechanism can be suggested based on the smearing of Fermi distributions in the contacts with temperature increase. In absence of external radiation extended tail of Fermi distribution at higher temperatures yields more electronic population closer to molecular resonance, which naturally leads to increase of electron flux. On the contrary, optical flux already being at resonance mostly depends on available electronic population at ground state. Smearing of Fermi distribution slightly diminishes the latter thus resulting in decrease of photo-induced current (see Fig. 3c). First principles simulations based on the proposed mechanism (see Fig. 3b) demonstrate qualitative correspondence with experimental data. We note that possible additional factor (not included into the model) decreasing photocurrent with temperature is scattering within the monolayer.[56]

Finally, we consider dependence of photocurrent on thickness of molecular layer. The consideration requires performing calculations for molecular chains of different lengths. In the analysis below we consider chains from $N = 1$ to $N = 5$ units. While dark current demonstrates exponential dependence on the layer size characteristic of tunneling, photocurrent practically does not depend on the thickness (see Fig. 4a). Such insensitivity is expected for hopping transport, and interplay between the two modes of behavior was discussed in the literature as result of competition between tunneling and thermally activated electron transfer via molecular bridges.[64–66] We suggest that the same mechanism is behind observed length dependence also in transport with a difference that optical excitation in present case
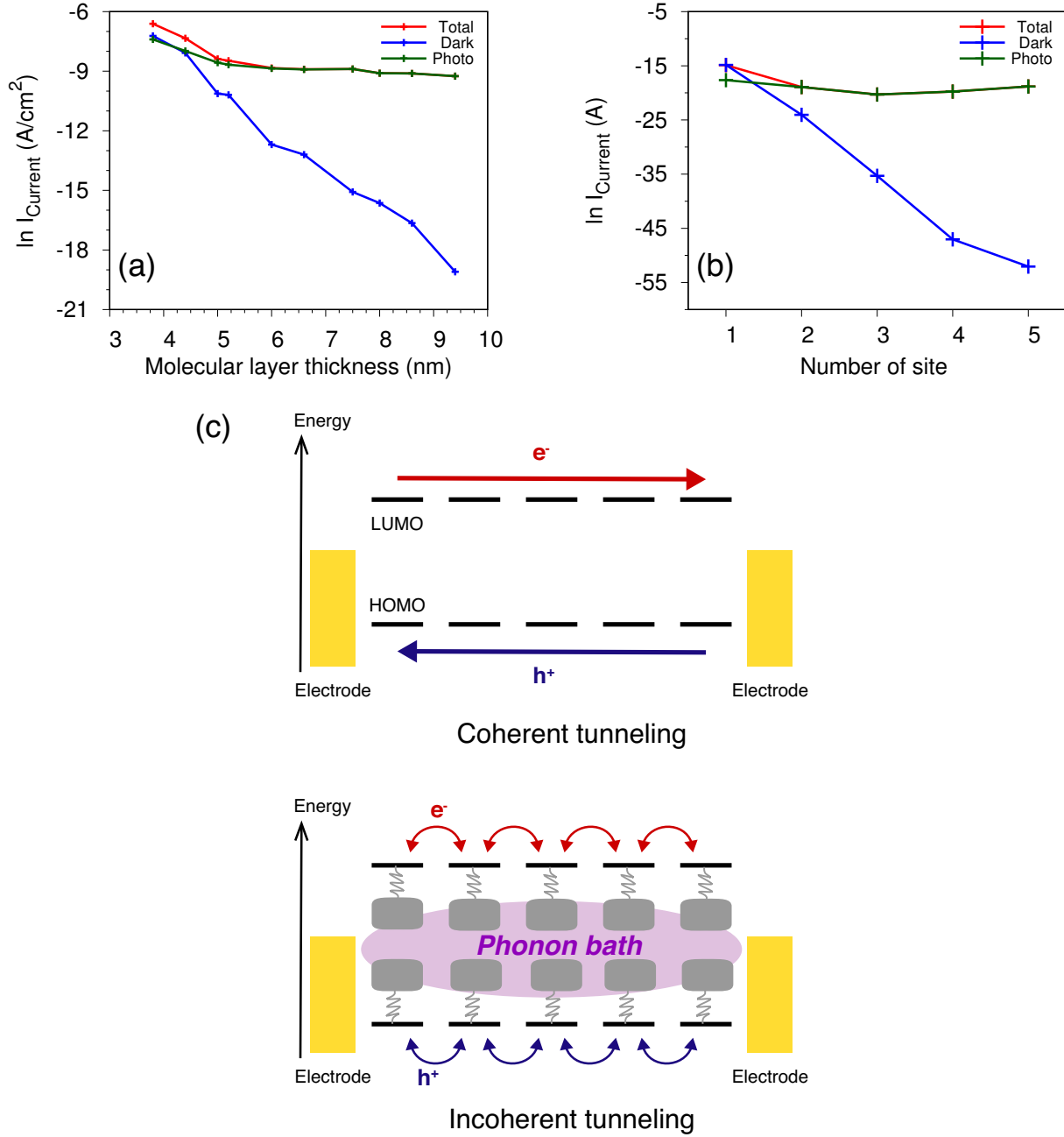
Figure 4: Dark (blue line), photo-induced (green line), and total (red line) currents vs. thickness of the molecular layer. Shown are (a) experimental data and (b) results of first-principles simulations within the Hubbard NEGF. Panel (c) shows sketch of the mechanism. Simulations are performed under constant bias of $V_{sd} = 0.02$ eV and external field illumination at wavelength $\lambda = 380$ nm. See text for other parameters.

plays the role of thermal activation in previous study (see Fig. 4c).

Hopping character of electron transport is caused by local dephasing (e.g., due to interaction with low frequency vibrations of nearby molecules in the layer), which is usually modeled by introducing Buttiker probes. Following Ref.[67] we represent Buttiker probes by attaching set of oscillators to each many-body state of molecules

$$\hat{H}_P = \sum_{n=1}^{N} \sum_{\beta_n} \sum_{S_n \in M_n} \left(\omega_{S_n} \hat{b}_{\beta_n}^\dagger \hat{b}_{\beta_n} + B_{\beta_n} (\hat{b}_{\beta_n} + \hat{b}_{\beta_n}^\dagger) \hat{X}_{S_n S_n} \right) \tag{15}$$

and considering a limit of $\omega_{S_n} \to 0$ to restrict the effect of oscillators to pure dephasing.

We treat both inter-molecule coupling and interactions with Buttiker probes within second order of diagrammatic perturbation theory for the Hubbard NEGF.[60] This leads to appearance of two additional self-energies in the self-consistent scheme (see Supporting Information for details). The two interactions are characterized by inter-atomic electron tunneling parameters $t_{\mathcal{M}_1 \mathcal{M}_2}$ and dephasing rate

$$\gamma_P^{S_n}(\omega) = 2\pi \sum_{\beta_n} \left| B_{\beta_n} \right|^2 \delta(\omega - \omega_{\beta_n}) \tag{16}$$

which we consider within wide band approximation. In the simulations all inter-molecule hopping parameters are taken 0.01 eV, dephasing rates are assumed to be 0.02 eV.

Figure 4 compares experimental data (panel a) with results of simulation (panel b). Simulations are performed under bias $V_{sd} = 0.02$ eV and external field illumination at wavelength $\lambda = 380$ nm. In both graphs dark current demonstrates exponential dependence on thickness of molecular layer characteristic for off-resonant tunneling through wide barrier. Photocurrent shows insensitivity to barrier width, which is characteristic of hopping transport regime. We note that the inverse Arrhenius behavior for the photocurrent evident in Figure 3a indicates that the hopping is activationless.[56]

In summary, we presented combined experimental and theoretical study of response of nitroazobenzene molecular junctions to external illumination and applied bias. Experimentally

observed characteristic behavior of dark and photo-induced currents was modeled within new diagrammatic technique for the Hubbard NEGF. Being a nonequilibrum atomic limit tool (i.e. formulation employing many-body states of isolated molecule as a basis) the Hubbard NEGF readily allows incorporation of the results of quantum chemistry simulations into transport behavior. We used first principles simulations to model photocurrent behavior and propose mechanisms behind the observed junction responses. In particular, temperature dependence of the currents is explained by smearing Fermi-Dirac distribution in the contacts with temperature increase, which results in increase of dark current due to shifting electron tunneling energies closer to molecular resonances and decrease of photo-induced current due to diminished population in the ground state. We note that scattering within molecular layer is an additional factor reducing photocurrent, which was not included in the theoretical model. Also, exponential decrease of dark current with molecular layer thickness was explained as a manifestation of (off-resonant) tunneling through a barrier, while insensitivity of photo-induced current on barrier thickness was identified with hopping regime of transport.

Further development of the Hubbard NEGF theory, formulation of universal Hubbard NEGF code for multi-state considerations, and application it to simulation of signals beyond fluxes are goals of future research.

Acknowledgement

Supporting Information Available

The following files are available free of charge. Supporting information contains details on

first principle (TD)DFT simulations and short description of the Hubbard NEGF employed in transport modeling.

References

(1) Aviram, A.; Ratner, M. A. Molecular rectifiers. *Chem. Phys. Lett.* **1974**, *29*, 277–283.

(2) Nitzan, A.; Ratner, M. A. Electron Transport in Molecular Wire Junctions. *Science* **2003**, *300*, 1384–1389.

(3) Lindsay, S. M.; Ratner, M. A. Molecular Transport Junctions: Clearing Mists. *Advanced Materials* **2007**, *19*, 23–31.

(4) Tao, N. J. Electron transport in molecular junctions. *Nature Nanotechnology* **2006**, *1*, 173–181.

(5) Galperin, M.; Ratner, M. A.; Nitzan, A.; Troisi, A. Nuclear Coupling and Polarization in Molecular Transport Junctions: Beyond Tunneling to Function. *Science* **2008**, *319*, 1056–1060.

(6) Galperin, M.; Ratner, M. A.; Nitzan, A. Molecular transport junctions: vibrational effects. *J. Phys.: Condens. Matter* **2007**, *19*, 103201.

(7) Zhitenev, N. B.; Meng, H.; Bao, Z. Conductance of Small Molecular Junctions. *Phys. Rev. Lett.* **2002**, *88*, 226801.

(8) Dekker, H. Quantization of the linearly damped harmonic oscillator. *Phys. Rev. A* **1977**, *16*, 2126–2134.

(9) Bayman, A.; Hansma, P. K.; Kaska, W. C. Shifts and dips in inelastic-electron-tunneling spectra due to the tunnel-junction environment. *Phys. Rev. B* **1981**, *24*, 2449 – 2455.

(10) Hahn, J. R.; Lee, H. J.; Ho, W. Electronic Resonance and Symmetry in Single-Molecule Inelastic Electron Tunneling. *Phys. Rev. Lett.* **2000**, *85*, 1914 – 1917.

(11) Wang, W.; Lee, T.; Kretzschmar, I.; Reed, M. A. Inelastic Electron Tunneling Spectroscopy of an Alkanedithiol Self-Assembled Monolayer. *Nano Lett.* **2004**, *4*, 643–646.

(12) Smit, R. H. M.; Noat, Y.; Untiedt, C.; Lang, N. D.; van Hemert, M. C.; van Ruitenbeek, J. M. Measurement of the conductance of a hydrogen molecule. *Nature* **2002**, *419*, 906–909.

(13) Agrait, N.; Untiedt, C.; Rubio-Bollinger, G.; Vieira, S. Onset of Energy Dissipation in Ballistic Atomic Wires. *Phys. Rev. Lett.* **2002**, *88*, 216803.

(14) Zhang, J.; Fu, Y.; Chowdhury, M. H.; Lakowicz, J. R. Metal-Enhanced Single-Molecule Fluorescence on Silver Particle Monomer and Dimer: Coupling Effect between Metal Particles. *Nano Lett.* **2007**, *7*, 2101–2107.

(15) Wu, S. W.; Nazin, G. V.; Ho, W. Intramolecular photon emission from a single molecule in a scanning tunneling microscope. *Phys. Rev. B* **2008**, *77*, 205430.

(16) Yoon, H. P.; Maitani, M. M.; Cabarcos, O. M.; Cai, L.; Mayer, T. S.; Allara, D. L. Crossed-Nanowire Molecular Junctions: A New Multispectroscopy Platform for Conduction-Structure Correlations. *Nano Lett.* **2010**, *10*, 2897–2902.

(17) Ward, D. R.; Halas, N. J.; Ciszek, J. W.; Tour, J. M.; Wu, Y.; Nordlander, P.; Natelson, D. Simultaneous Measurements of Electronic Conduction and Raman Response in Molecular Junctions. *Nano Lett.* **2008**, *8*, 919–924.

(18) Ioffe, Z.; Shamai, T.; Ophir, A.; Noy, G.; Yutsis, I.; Kfir, K.; Cheshnovsky, O.; Selzer, Y. Detection of heating in current-carrying molecular junctions by Raman scattering. *Nature Nanotech.* **2008**, *3*, 727–732.

(19) Ward, D. R.; Corley, D. A.; Tour, J. M.; Natelson, D. Vibrational and electronic heating in nanoscale junctions. *Nature Nanotech.* **2011**, *6*, 33–38.

(20) Kim, K.; Choi, J.-Y.; Lee, H. B.; Shin, K. S. Raman scattering of 4-aminobenzenethiol sandwiched between Ag nanoparticle and macroscopically smooth Au substrate: Effects of size of Ag nanoparticles and the excitation wavelength. *The Journal of Chemical Physics* **2011**, *135*, 124705.

(21) Shamai, T.; Selzer, Y. Spectroscopy of molecular junctions. *Chem. Soc. Rev.* **2011**, *40*, 2293–2305.

(22) Banik, M.; El-Khoury, P. Z.; Nag, A.; Rodriguez-Perez, A.; Guarrottxena, N.; Bazan, G. C.; Apkarian, V. A. Surface-Enhanced Raman Trajectories on a Nano-Dumbbell: Transition from Field to Charge Transfer Plasmons as the Spheres Fuse. *ACS Nano* **2012**, *6*, 10343–10354.

(23) Zhang, R.; Zhang, Y.; Dong, Z. C.; Jiang, S.; Zhang, C.; Chen, L. G.; Zhang, L.; Liao, Y.; Aizpurua, J.; Luo, Y.; Yang, J. L.; Hou, J. G. Chemical mapping of a single molecule by plasmon-enhanced Raman scattering. *Nature* **2013**, *498*, 82–86.

(24) Ward, D. R.; Grady, N. K.; Levin, C. S.; Halas, N. J.; Wu, Y.; Nordlander, P.; Natelson, D. Electromigrated Nanoscale Gaps for Surface-Enhanced Raman Spectroscopy. *Nano Lett.* **2007**, *7*, 1396–1400.

(25) Arielly, R.; Ofarim, A.; Noy, G.; Selzer, Y. Accurate Determination of Plasmonic Fields in Molecular Junctions by Current Rectification at Optical Frequencies. *Nano Lett.* **2011**, *11*, 2968–2972.

(26) Vadai, M.; Nachman, N.; Ben-Zion, M.; Bürkle, M.; Pauly, F.; Cuevas, J. C.; Selzer, Y. Plasmon-Induced Conductance Enhancement in Single-Molecule Junctions. *J. Phys. Chem. Lett.* **2013**, *4*, 2811–2816.

(27) Dey, S.; Mirell, D.; Perez, A. R.; Lee, J.; Apkarian, V. A. Nonlinear femtosecond laser induced scanning tunneling microscopy. *The Journal of Chemical Physics* **2013**, *138*, –.

(28) Evans, K. M.; Zolotavin, P.; Natelson, D. Plasmon-Assisted Photoresponse in Ge-Coated Bowtie Nanojunctions. *ACS Photonics* **2015**, *2*, 1192–1198.

(29) Schneider, N. L.; Schull, G.; Berndt, R. Optical Probe of Quantum Shot-Noise Reduction at a Single-Atom Contact. *Phys. Rev. Lett.* **2010**, *105*, 026601.

(30) Schneider, N. L.; Lü, J. T.; Brandbyge, M.; Berndt, R. Light Emission Probing Quantum Shot Noise and Charge Fluctuations at a Biased Molecular Junction. *Phys. Rev. Lett.* **2012**, *109*, 186601.

(31) Imada, H.; Miwa, K.; Imai-Imada, M.; Kawahara, S.; Kimura, K.; Kim, Y. Real-space investigation of energy transfer in heterogeneous molecular dimers. *Nature* **2016**, *538*, 364–367.

(32) Imada, H.; Miwa, K.; Imai-Imada, M.; Kawahara, S.; Kimura, K.; Kim, Y. Single-Molecule Investigation of Energy Dynamics in a Coupled Plasmon-Exciton System. *Phys. Rev. Lett.* **2017**, *119*, 013901.

(33) Sonntag, M. D.; Chulhai, D.; Seideman, T.; Jensen, L.; Duyne, R. P. V. The Origin of Relative Intensity Fluctuations in Single-Molecule Tip-Enhanced Raman Spectroscopy. *Journal of the American Chemical Society* **2013**, *135*, 17187–17192.

(34) El-Khoury, P. Z.; Hu, D.; Apkarian, V. A.; Hess, W. P. Raman Scattering at Plasmonic Junctions Shorted by Conductive Molecular Bridges. *Nano Letters* **2013**, *13*, 1858–1861.

(35) Yampolsky, S.; Fishman, D. A.; Dey, S.; Hulkko, E.; Banik, M.; Potma, E. O.; Apkar-

ian, V. A. Seeing a single molecule vibrate through time-resolved coherent anti-Stokes Raman scattering. *Nat. Photon.* **2014**, *8*, 650–656.

(36) Arielly, R.; Vadai, M.; Kardash, D.; Noy, G.; Selzer, Y. Real-Time Detection of Redox Events in Molecular Junctions. *Journal of the American Chemical Society* **2014**, *136*, 2674–2680.

(37) Pozzi, E. A.; Sonntag, M. D.; Jiang, N.; Klingsporn, J. M.; Hersam, M. C.; Duyne, R. P. V. Tip-Enhanced Raman Imaging: An Emergent Tool for Probing Biology at the Nanoscale. *ACS Nano* **2013**, *7*, 885–888.

(38) Klingsporn, J. M.; Sonntag, M. D.; Seideman, T.; Van Duyne, R. P. Tip-Enhanced Raman Spectroscopy with Picosecond Pulses. *J. Phys. Chem. Lett.* **2014**, *5*, 106–110, PMID: 26276188.

(39) Pozzi, E. A.; Sonntag, M. D.; Jiang, N.; Chiang, N.; Seideman, T.; Hersam, M. C.; Duyne, R. P. V. Ultrahigh Vacuum Tip-Enhanced Raman Spectroscopy with Picosecond Excitation. *The Journal of Physical Chemistry Letters* **2014**, *5*, 2657–2661.

(40) Kurouski, D.; Mattei, M.; Van Duyne, R. P. Probing Redox Reactions at the Nanoscale with Electrochemical Tip-Enhanced Raman Spectroscopy. *Nano Lett.* **2015**, *15*, 7956–7962, PMID: 26580153.

(41) Grosse, C.; Etzkorn, M.; Kuhnke, K.; Loth, S.; Kern, K. Quantitative mapping of fast voltage pulses in tunnel junctions by plasmonic luminescence. *Appl. Phys. Lett.* **2013**, *103*, 183108.

(42) Jahng, J.; Brocious, J.; Fishman, D. A.; Yampolsky, S.; Nowak, D.; Huang, F.; Apkarian, V. A.; Wickramasinghe, H. K.; Potma, E. O. Ultrafast pump-probe force microscopy with nanoscale resolution. *Applied Physics Letters* **2015**, *106*, –.

(43) Jiang, N.; Foley, E. T.; Klingsporn, J. M.; Sonntag, M. D.; Valley, N. A.; Dieringer, J. A.; Seideman, T.; Schatz, G. C.; Hersam, M. C.; Van Duyne, R. P. Observation of Multiple Vibrational Modes in Ultrahigh Vacuum Tip-Enhanced Raman Spectroscopy Combined with Molecular-Resolution Scanning Tunneling Microscopy. *Nano Lett.* **2012**, *12*, 5061–5067, PMID: 22200250.

(44) Lee, J.; Perdue, S. M.; Perez, A. R.; Apkarian, V. A. Vibronic Motion with Joint Angstrom-Femtosecond Resolution Observed through Fano Progressions Recorded within One Molecule. *ACS Nano* **2014**, *8*, 54–63, PMID: 24261832.

(45) Herzog, J. B.; Knight, M. W.; Natelson, D. Thermoplasmonics: Quantifying Plasmonic Heating in Single Nanowires. *Nano Letters* **2014**, *14*, 499–503.

(46) Pozzi, E. A.; Zrimsek, A. B.; Lethiec, C. M.; Schatz, G. C.; Hersam, M. C.; Van Duyne, R. P. Evaluating Single-Molecule Stokes and Anti-Stokes SERS for Nanoscale Thermometry. *J. Phys. Chem. C* **2015**, *119*, 21116–21124.

(47) Nardin, G.; Autry, T. M.; Silverman, K. L.; Cundiff, S. T. Multidimensional coherent photocurrent spectroscopy of a semiconductor nanostructure. *Opt. Express* **2013**, *21*, 28617–28627.

(48) Karki, K. J.; Widom, J. R.; Seibt, J.; Moody, I.; Lonergan, M. C.; Pullerits, T.; Marcus, A. H. Coherent two-dimensional photocurrent spectroscopy in a PbS quantum dot photocell. *Nat. Commun.* **2014**, *5*, 5869.

(49) Vella, E.; Li, H.; Grégoire, P.; Tuladhar, S. M.; Vezie, M. S.; Few, S.; Bazán, C. M.; Nelson, J.; Silva-Acuña, C.; Bittner, E. R. Ultrafast decoherence dynamics govern photocarrier generation efficiencies in polymer solar cells. *Sci. Rep.* **2016**, *6*, 29437–.

(50) Fereiro, J. A.; Kondratenko, M.; Bergren, A. J.; McCreery, R. L. Internal Photoemission in Molecular Junctions: Parameters for Interfacial Barrier Determinations. *J. Am. Chem. Soc.* **2015**, *137*, 1296–1304, PMID: 25562564.

(51) Pourhossein, P.; Vijayaraghavan, R. K.; Meskers, S. C. J.; Chiechi, R. C. Optical modulation of nano-gap tunnelling junctions comprising self-assembled monolayers of hemicyanine dyes. *Nat. Commun.* **2016**, *7*, 11749.

(52) Ivashenko, O.; Bergren, A. J.; McCreery, R. L. Monitoring of Energy Conservation and Losses in Molecular Junctions through Characterization of Light Emission. *Adv. Electron. Mater.* **2016**, *2*, 1600351.

(53) Ivashenko, O.; Bergren, A. J.; McCreery, R. L. Light Emission as a Probe of Energy Losses in Molecular Junctions. *J. Am. Chem. Soc.* **2016**, *138*, 722–725, PMID: 26745544.

(54) Du, W.; Wang, T.; Chu, H.-S.; Wu, L.; Liu, R.; Sun, S.; Phua, W. K.; Wang, L.; Tomczak, N.; Nijhuis, C. A. On-chip molecular electronic plasmon sources based on self-assembled monolayer tunnel junctions. *Nat. Photon.* **2016**, *10*, 274–280.

(55) Tefashe, U. M.; Nguyen, Q. V.; Lafolet, F.; Lacroix, J.-C.; McCreery, R. L. Robust Bipolar Light Emission and Charge Transport in Symmetric Molecular Junctions. *J. Am. Chem. Soc.* **2017**, *139*, 7436–7439, PMID: 28528551.

(56) Najarian, A. M.; McCreery, R. L. Long-Range Activationless Photostimulated Charge Transport in Symmetric Molecular Junctions. *ACS Nano* **2019**, *13*, 867–877.

(57) Morteza Najarian, A.; Bayat, A.; McCreery, R. L. Orbital Control of Photocurrents in Large Area All-Carbon Molecular Junctions. *J. Am. Chem. Soc.* **2018**, *140*, 1900–1909, PMID: 29319313.

(58) Galperin, M.; Nitzan, A. Molecular optoelectronics: The interaction of molecular conduction junctions with light. *Phys. Chem. Chem. Phys.* **2012**, *14*, 9421–9438.

(59) Galperin, M. Photonics and spectroscopy in nanojunctions: a theoretical insight. *Chem. Soc. Rev.* **2017**, *46*, 4000–4019.

(60) Chen, F.; Ochoa, M. A.; Galperin, M. Nonequilibrium diagrammatic technique for Hubbard Green functions. *J. Chem. Phys.* **2017**, *146*, 092301.

(61) Miwa, K.; Chen, F.; Galperin, M. Towards Noise Simulation in Interacting Nonequilibrium Systems Strongly Coupled to Baths. *Scientific Reports* **2017**, *7*, 9735.

(62) Haug, H.; Jauho, A.-P. *Quantum Kinetics in Transport and Optics of Semiconductors*, second, substantially revised edition ed.; Springer: Berlin Heidelberg, 2008.

(63) Galperin, M.; Nitzan, A. Current-Induced Light Emission and Light-Induced Current in Molecular-Tunneling Junctions. *Phys. Rev. Lett.* **2005**, *95*, 206802.

(64) Segal, D.; Nitzan, A.; Davis, W. B.; Wasielewski, M. R.; Ratner, M. A. Electron Transfer Rates in Bridged Molecular Systems 2. A Steady-State Analysis of Coherent Tunneling and Thermal Transitions. **2000**, *104*, 3817–3829.

(65) Ho Choi, S.; Kim, B.; Frisbie, C. D. Electrical Resistance of Long Conjugated Molecular Wires. *Science* **2008**, *320*, 1482–1486.

(66) Choi, S. H.; Risko, C.; Delgado, M. C. R.; Kim, B.; BrÃľdas, J.-L.; Frisbie, C. D. Transition from Tunneling to Hopping Transport in Long, Conjugated Oligo-imine Wires Connected to Metals. *Journal of the American Chemical Society* **2010**, *132*, 4358–4368, PMID: 20218660.

(67) White, A. J.; Peskin, U.; Galperin, M. Coherence in charge and energy transfer in molecular junctions. *Phys. Rev. B* **2013**, *88*, 205424.

Graphical TOC Entry